

# Experimental construction of a symmetric three-qubit entangled state and its utility in testing the violation of a Bell inequality on an NMR quantum simulator

Dileep Singh,<sup>1,\*</sup> Vaishali Gulati,<sup>1,†</sup> Arvind,<sup>1,2,‡</sup> and Kavita Dorai<sup>1,§</sup>

<sup>1</sup>*Department of Physical Sciences, Indian Institute of Science Education & Research Mohali, Sector 81 SAS Nagar, Manauli PO 140306 Punjab, India.*

<sup>2</sup>*Vice Chancellor, Punjabi University Patiala, 147002, Punjab, India*

We designed a quantum circuit to prepare a permutation-symmetric maximally entangled three-qubit state called the  $|S\rangle$  state and experimentally created it on an NMR quantum processor. The presence of entanglement in the state was certified by computing two different entanglement measures, namely negativity and concurrence. We used the  $|S\rangle$  state in conjunction with a set of maximally incompatible local measurements, to demonstrate the maximal violation of inequality number 26 in Sliwa's classification scheme, which is a tight Bell inequality for the (3,2,2) scenario i.e. the three party, two measurement settings and two measurement outcomes scenario.

## I. INTRODUCTION

Entanglement is intrinsic to quantum systems and its production, characterization and protection have been well studied, with a view to using it as a resource for quantum information processing [1]. Three-qubit entanglement has been extensively characterized and it was showed that three qubits can be entangled in two inequivalent ways [2, 3]. Permutation symmetric entangled states i.e. states that remain invariant under pair-wise qubit swapping, have been proven to be useful for a wide variety of quantum information tasks [4–6]. The entanglement of symmetric multipartite states was characterized using a geometric entanglement measure [7, 8], and quantum circuits were proposed to efficiently construct genuinely entangled permutation-invariant multipartite quantum states [9].

It is important to design experimental schemes to generate and characterize different kinds of multipartite entangled states. In this context, our previous work on three-qubit entanglement focused on experimentally implementing a canonical form for three-qubit pure states, from which all other states can be constructed, including the GHZ and W entangled states [10]. Interestingly, we were able to show that for nearly all pure states (except those belonging to the GHZ class), the two-qubit reduced states were sufficient to reconstruct the whole three-qubit state. We experimentally constructed a novel three-qubit entangled  $W\bar{W}$  state, which is interconvertible with the GHZ state, but stores information about multipartite correlations in a totally different way [11]. While studying the decoherence of entangled states, we found that the GHZ-class of states are the most fragile, while the W-class of states are the most robust against the natural noise present in the NMR system [12].

Nonlocal correlations in a spatially separated multi-

partite quantum system have an inherent measurement statistics which is not classically reproducible [13] and their presence can be revealed via the violation of Bell-type inequalities such as the Clauser-Horne-Shimony-Holt (CHSH) inequality [14]. Nonlocality has potential applications in secure communication [15] and quantum information [16].  $N$ -partite generalization of Wigner's argument was used to obtain a Bell-type inequality and its violation by GHZ, Cluster and W states was investigated [17]. Nonlocality of three-qubit pure states has been explored by looking at the violation of the CHSH inequality [18–20]. Entanglement has to be present in the state for nonlocal correlations to exist [21], and several studies have focused on understanding the connection between nonlocality and entanglement [22–24]. Incompatibility is another important property of quantum systems which states that the outcome of certain observables cannot be obtained simultaneously [25]. Incompatibility of measurements is necessary for the violation of any Bell inequality [26–28]. It was demonstrated that measurement compatibility can be used to both detect Bell nonlocality and to certify entanglement in a device-independent manner [29]. The question of how incompatible the measurements have to be in order to achieve a violation of a Bell inequality was explored and quantifiers of measurement incompatibility were devised [30]. The (3,2,2) scenario i.e. the three party, two measurement settings per party and two measurement outcomes scenario provides detailed information about the combination of entanglement and incompatibility that could lead to maximal nonlocality for tight Bell inequalities [31]. Only Bell, GHZ and  $|S\rangle$  states produce maximal violation of a tight Bell inequality via maximally incompatible measurements [32, 33]. The experimental demonstration of the maximum quantum violation of tight Bell inequalities with GHZ and Bell and the  $|S\rangle$  states has been demonstrated using a photonic set-up [34–36] as well with ion traps [37].

In this work, we designed and experimentally implemented a quantum circuit to prepare the three-qubit symmetric entangled  $|S\rangle$  state on an NMR quantum processor. We certified the entanglement of the  $|S\rangle$  state

\* dileepsingh@iisermohali.ac.in

† vaishaligulati00@gmail.com

‡ arvind@iisermohali.ac.in

§ kavita@iisermohali.ac.in

by calculating the experimental values of the tripartite negativity and the concurrence. We then demonstrated the utility of the  $|S\rangle$  state by experimentally simulating the violation of the tight Bell inequality (number 26 in Sliwa's classification scheme) in the  $(3, 2, 2)$  scenario [31]. Maximal incompatibility was checked by adding compatible measurements in the existing measurement setting. We refer to our experiment as a "simulation", since in an NMR set-up, the qubits are realized by nuclear spins bound in the same molecule and separated by a few angstroms, so there is no actual spatial separation or nonlocality [38].

The material in this paper is arranged as follows: Section II briefly describes the theoretical framework of the entanglement properties of the  $|S\rangle$  state and the maximal quantum violation of the tight Bell inequality using the entangled  $|S\rangle$  state. Section III describes the experimental construction of the entangled  $|S\rangle$  state and the simulation of the violation of the tight Bell inequality, inequality number 26 in Sliwa's classification in the  $(3, 2, 2)$  scenario, on a three-qubit NMR quantum computer. The NMR experimental details are summarized in Section III A and the details of the quantum circuit and NMR pulse sequence to construct the  $|S\rangle$  state are given in Section III B. The experimental certification of the presence of entanglement in the  $|S\rangle$  state is given in Section III C. The results of the experimental violation of the inequality are given in Section III D. Section IV contains a few concluding remarks.

## II. THEORETICAL BACKGROUND

Three-qubit entanglement with genuine three-party entanglement, has been well studied and falls into one of the two inequivalent classes namely, the GHZ class and the W class [2]. The  $|S\rangle$  state which is a three-qubit permutation-symmetric entangled state, has been defined as [31]:

$$|S\rangle = \frac{1}{\sqrt{6}}(|001\rangle + |010\rangle - |100\rangle) + \frac{1}{\sqrt{2}}|111\rangle \quad (1)$$

The  $|S\rangle$  belongs to the W class of states and therefore is inequivalent to the GHZ state under local operations and classical communication (LOCC). The qubit-qubit concurrences for this state are all equal to 0.244, as opposed to the W state whose qubit-qubit concurrences are all equal to 0.667 [36]. The  $|S\rangle$  state has interesting properties and as we shall see, plays an important role in the context of violation of Bell's inequalities for the  $(3,2,2)$  scenario.

Quantum nonlocality has been classified according to the combinations of entangled states and incompatible measurements for 46 classes of tight Bell inequalities in the  $(3,2,2)$  scenario [31]. The inequality number 26 in

Sliwa's classification scheme is given by:

$$\begin{aligned} T_{26} = & \langle A_0 \rangle + \langle B_0 \rangle + \langle A_0 B_0 \rangle + 2\langle A_1 B_1 \rangle + \langle C_0 \rangle \\ & + \langle A_0 C_0 \rangle + \langle B_0 C_0 \rangle - \langle A_0 B_0 C_0 \rangle - 2\langle A_1 B_1 C_0 \rangle \\ & + 2\langle A_1 C_1 \rangle - 2\langle A_1 B_0 C_1 \rangle - 2\langle B_1 C_1 \rangle \\ & + \langle A_0 B_1 C_1 \rangle \leq 5 \end{aligned} \quad (2)$$

where  $A_i, B_i, C_i$  are the measurement settings of the first, second and third party, respectively. Each observable is dichotomous and can have  $\pm 1$  outcomes. The maximum quantum violation of the inequality number 26 in Sliwa's classification scheme is achieved using the entangled  $|S\rangle$  state given in Eq. 1 [39].

For the particular set of observables  $A_0 = B_0 = C_0 = \sigma_z$  and  $A_1 = B_1 = C_1 = \sigma_x$  which are maximally incompatible according to any quantifier of incompatibility, the  $|S\rangle$  state produces the maximum quantum violation given by [31]:

$$T_{26} = 1 + 4\sqrt{3} \approx 7.928 \quad (3)$$

## III. EXPERIMENTAL CONSTRUCTION OF $|S\rangle$ STATE AND VIOLATION OF BELL INEQUALITY

### A. NMR experimental details

We used the molecule iodotrifluoroethylene dissolved in acetone-d6 with the three ( $^{19}\text{F}$ ) spins encoding the three NMR qubits. The molecular structure and other experimental details are given in Ref. [12]. The three-qubit Hamiltonian in a rotating frame is given by:

$$H = -\sum_{i=1}^3 (\omega_i - \omega_{RF}) I_{iz} + \sum_{i>j,j=1}^3 2\pi J_{ij} I_{iz} I_{jz} \quad (4)$$

where  $I_{iz}, \omega_i, J_{ij}$  denote the spin angular momentum operator, the Larmor frequencies, and the scalar coupling constants, respectively. The first term in the Hamiltonian represents the Zeeman interaction between the spins and the applied static magnetic field, while the second term represents the interaction term. More details are provided in Ref [40].

The NMR experiments were performed at room temperature and the system was initialized in a pseudopure (PPS) state, which mimics a pure state [40, 41]. The PPS state  $|000\rangle$  was achieved via the spatial averaging technique [42] with the density operator being given by:

$$\rho_{000} = \frac{1-\epsilon}{8} I_8 + \epsilon |000\rangle\langle 000| \quad (5)$$

where  $I_8$  is the  $8 \times 8$  identity operator and  $\epsilon$  is proportional to the spin polarization which is  $\approx 10^{-5}$  at room temperature.

The NMR pulse sequence for preparing the PPS state  $|000\rangle$  can be found in Ref. [12] which gives details of the

specific sequence of RF pulses, four Z gradient pulses, and three time evolution periods that are used. We used the Gradient Ascent Pulse Engineering (GRAPE) technique [43, 44] for the optimization of all the RF pulses used to construct the PPS state. The GRAPE optimized RF pulses are robust against RF inhomogeneity, with an average fidelity of  $\geq 0.999$ . We used four GRAPE pulses ( $U_{P1}, U_{P2}, U_{P3}, U_{P4}$ ) optimized to reach the PPS state from the thermal state, where some RF pulses were combined into a single pulse. The duration of pulses  $U_{P1}, U_{P2}, U_{P3}, U_{P4}$  are  $500\mu s, 9000\mu s, 7500\mu s, 4000\mu s$  respectively. The experimental state was reconstructed using a least squares constrained convex optimization technique [45]. The set of tomographic operations  $\{III, IYY, IYY, YII, XYX, XXY, XXX\}$  where the  $X(Y)$  denotes the single spin operator implemented by a spin-selective  $\frac{\pi}{2}$  pulse and  $I$  denotes no operation were performed to reconstruct the final density operator. All the seven tomography spin selective pulses were optimized using GRAPE with the length of each pulse being  $\approx 500\mu s$ . The PPS state  $|000\rangle$  had an experimental state fidelity of 0.997.

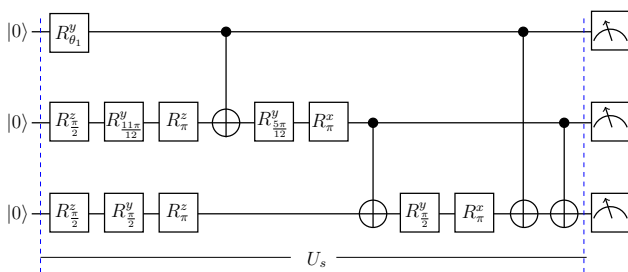


FIG. 1. Quantum circuit showing the sequence of implementation of the single-qubit local rotation gates and two-qubit controlled-NOT gates required to construct the  $|S\rangle$  state from the PPS state  $|000\rangle$  state.  $U_s$  denotes the complete unitary including all quantum gates used for the state preparation.

### B. Experimental construction of the $|S\rangle$ state

After preparing the PPS state, we turn to the experimental preparation of the tripartite  $|S\rangle$  state on the three-qubit NMR system. The quantum circuit to prepare the  $|S\rangle$  state starting from the PPS  $|000\rangle$  state. is given in Fig. 1. The quantum circuit contains several one-qubit gates and two-qubit gates. The NMR pulse sequence corresponding to the quantum circuit is shown in Fig. 2. All the NMR pulses were numerically optimized using the GRAPE algorithm and we were able to achieve high gate fidelities with relatively small RF pulse durations. The unitary operator for the entire preparation sequence of Fig. 2 contains four CNOT gates and eleven non-selective rotations; the entire unitary was generated by a specially crafted single GRAPE pulse  $U_s$  having a duration of  $\approx 4600\mu s$ .

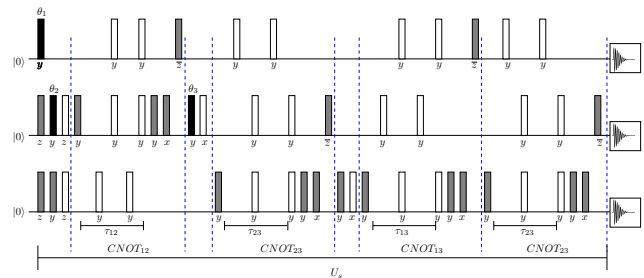


FIG. 2. NMR pulse sequence corresponding the quantum circuit used to prepare the  $|S\rangle$  state starting from the PPS state. The black rectangles denote RF pulse rotations with  $\theta_1 = \frac{1.216\pi}{2}$ ,  $\theta_2 = \frac{11\pi}{12}$  and  $\theta_3 = \frac{5\pi}{12}$ . Grey rectangles denote  $\frac{\pi}{2}$  rotations and unfilled rectangles denote  $\pi$  rotations. The phase of each pulse is written below each rectangle. The time intervals are set to  $\tau_{12} = \frac{1}{2J_{12}}$ ,  $\tau_{13} = \frac{1}{2J_{13}}$ ,  $\tau_{23} = \frac{1}{2J_{23}}$  with  $J_{12} = 69.65$  Hz,  $J_{13} = 47.67$  Hz,  $J_{23} = -128.23$  Hz. The blue dotted lines separate the pulses achieving each CNOT gate and the total combination of all the gates is denoted by a single unitary  $U_s$ .

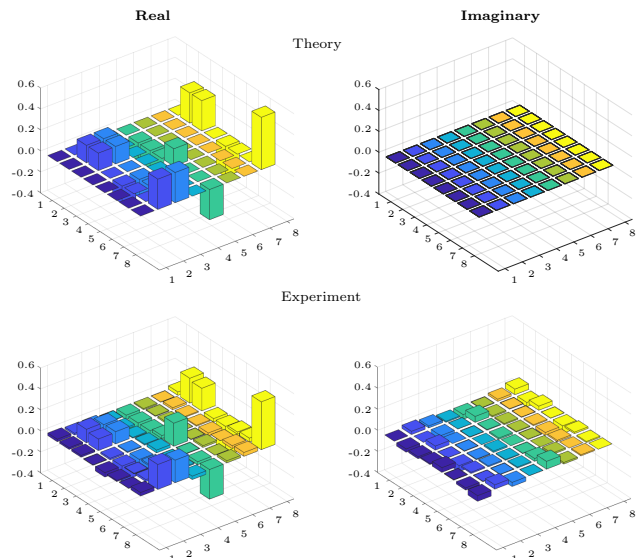


FIG. 3. The real (left) and imaginary (right) parts of the theoretical and experimental tomographs of the  $|S\rangle$  state. The labels 1, 2, 3, ..., 8 represent rows and columns encoding the computational basis in binary order from  $|000\rangle$  to  $|111\rangle$ .

To check the quality of the prepared  $|S\rangle$  state, state tomography was performed using the least squares optimization technique and an experimental state fidelity of  $0.949 \pm 0.003$  was obtained. The tomographs of the  $|S\rangle\langle S|$  state are shown in Fig. 3.

### C. Entanglement verification of the $|S\rangle$ state

Next, we experimentally verified the entanglement of the  $|S\rangle$  state. To quantify entanglement, we used the

well-known tripartite negativity measure [46]. The tripartite negativity can be calculated using the bipartite negativity, where bipartite negativity is the absolute value of the sum of the negative eigenvalues of  $\rho^{T_A}$  with  $T_A$  denoting the partial transpose of  $\rho$  with respect to the subsystem  $A$  in the bipartition  $A|BC$ . Negativity is zero if the partial transpose  $\rho^{T_A}$  has no negative eigenvalues. Tripartite negativity  $N$  then becomes  $(N_{A|BC}N_{B|AC}N_{C|BA})^{\frac{1}{3}}$ . It ranges from 0 for a separable state to 1 at the maximally entangled state. We computed the tripartite negativity for the experimentally prepared  $|S\rangle$  state and obtained  $N = 0.794 \pm 0.015$ , which is close to the theoretically predicted value of 0.943. This clearly shows the presence of tripartite entanglement in the  $|S\rangle$  state.

We also verified the entanglement of the  $|S\rangle$  state by using another entanglement measure termed qubit-qubit concurrence [47]. The concurrence is calculated from the eigenvalues  $\lambda_1 \geq \lambda_2 \geq \lambda_3 \geq \lambda_4$  of the matrix  $R = \rho(\sigma_y \otimes \sigma_y)\rho^*(\sigma_y \otimes \sigma_y)$  where  $\sigma_y$  is the Pauli matrix and  $\rho$  and  $\rho^*$  denote the density matrix and its complex conjugate, respectively. The qubit-qubit concurrence is given by  $C(\rho) = \max(0, \sqrt{\lambda_1} - \sqrt{\lambda_2} - \sqrt{\lambda_3} - \sqrt{\lambda_4})$ . The bipartite concurrence ranges between 0 and 1, with 0 implying no entanglement is present in the system and 1 indicating maximal entanglement. The experimental values we obtained for the qubit-qubit concurrence, range from  $\approx 0.094 - 0.32$ , which verifies the presence of entanglement in the  $|S\rangle$  state.

#### D. Inequality violation

The experimentally prepared  $|S\rangle$  state was used to test the inequality  $T_{26}$  defined in Eqn 2. The numerical value of experimental violation we obtain is:

$$T_{26} = 6.531 \pm 0.125 \quad (6)$$

where the observables  $A_0 = B_0 = C_0 = \sigma_z$  and  $A_1 = B_1 = C_1 = \sigma_x$  are maximally incompatible for each of the three parties.

In addition, we checked the maximal incompatibility of the observables of the three parties by changing one of the observables out of the six local measurements while leaving the other five in their initial configuration. These measurement modifications led to a decrease in the inequality value of  $T_{26}$ , fulfilling the requirement of maximal incompatibility in the three parties for the  $T_{26}$  scenario.

#### IV. CONCLUSIONS

We experimentally prepared the genuinely entangled three-qubit state  $|S\rangle$  on an NMR quantum processor, and certified its entanglement using two different entanglement measures namely, negativity, and qubit-qubit concurrence. We used the  $|S\rangle$  state to experimentally simulate the maximum quantum violation of a tripartite tight Bell inequality. Our results show a clear violation of the tight Bell inequality, revealing the maximally non-local behavior. We also tested the maximal incompatibility of the observables by modifying one of the six observables. An NMR quantum processor is a good testbed to perform tests of foundational issues in quantum mechanics. Our results are a step forward in the direction of unearthing deeper connections between nonlocality, entanglement, and incompatibility.

#### ACKNOWLEDGMENTS

All the experiments were performed on a Bruker Avance-III 400 MHz FT-NMR spectrometer at the NMR Research Facility of IISER Mohali. A. acknowledges financial support from DST/ICPS/QuST/Theme-1/2019/Q-68. K. D. acknowledges financial support from DST/ICPS/QuST/Theme-2/2019/Q-74.

- 
- [1] R. Horodecki, P. Horodecki, M. Horodecki, and K. Horodecki, *Rev. Mod. Phys.* **81**, 865 (2009).
  - [2] W. Dür, G. Vidal, and J. I. Cirac, *Phys. Rev. A* **62**, 062314 (2000).
  - [3] C. Sabin and G. Garcia-Alcaine, *The European Physical Journal D* **48**, 435 (2008).
  - [4] M. Hayashi, D. Markham, M. Muraio, M. Owari, and S. Virmani, *Phys. Rev. A* **77**, 012104 (2008).
  - [5] G. Toth and O. Gühne, *Phys. Rev. Lett.* **102**, 170503 (2009).
  - [6] P. Mathonet, S. Krins, M. Godefroid, L. Lamata, E. Solano, and T. Bastin, *Phys. Rev. A* **81**, 052315 (2010).
  - [7] M. Aulbach, D. Markham, and M. Muraio, *New Journal of Physics* **12**, 073025 (2010).
  - [8] M. AULBACH, *International Journal of Quantum Information* **10**, 1230004 (2012), <https://doi.org/10.1142/S0219749912300045>.
  - [9] A. Burchardt, J. Czartowski, and K. Życzkowski, *Phys. Rev. A* **104**, 022426 (2021).
  - [10] S. Dogra, K. Dorai, and Arvind, *Phys. Rev. A* **91**, 022312 (2015).
  - [11] D. Das, S. Dogra, K. Dorai, and Arvind, *Phys. Rev. A* **92**, 022307 (2015).
  - [12] H. Singh, Arvind, and K. Dorai, *Phys. Rev. A* **97**, 022302 (2018).
  - [13] J. S. Bell, *Physics* **1**, 195 (1964).
  - [14] A. Peres, *Foundations of Physics* **29**, 589 (1999).
  - [15] H. Buhrman, R. Cleve, S. Massar, and R. de Wolf, *Rev. Mod. Phys.* **82**, 665 (2010).

- [16] Z.-B. Chen, G. Hou, and Y.-D. Zhang, *Phys. Rev. A* **65**, 032317 (2002).
- [17] D. Home, D. Saha, and S. Das, *Phys. Rev. A* **91**, 012102 (2015).
- [18] H. Ozeki and S. Ishizaka, *Int. J. Quant. Inf.* **18**, 2050014 (2020), <https://doi.org/10.1142/S0219749920500148>.
- [19] K. Anjali, A. S. Hejamadi, H. S. Karthik, S. Sahu, Sudha, and A. R. U. Devi, *Quant. Inf. Process.* **20**, 187 (2021).
- [20] L. Tendick, H. Kampermann, and D. Bruß, *Phys. Rev. Research* **4**, L012002 (2022).
- [21] Y.-C. Liang, T. Vértesi, and N. Brunner, *Phys. Rev. A* **83**, 022108 (2011).
- [22] R. F. Werner, *Phys. Rev. A* **40**, 4277 (1989).
- [23] A. Acín, N. Gisin, and B. Toner, *Phys. Rev. A* **73**, 062105 (2006).
- [24] D. Cavalcanti, L. Guerini, R. Rabelo, and P. Skrzypczyk, *Phys. Rev. Lett.* **117**, 190401 (2016).
- [25] T. Heinosaari, J. Kiukas, and D. Reitzner, *Phys. Rev. A* **92**, 022115 (2015).
- [26] R. Uola, T. Moroder, and O. Gühne, *Phys. Rev. Lett.* **113**, 160403 (2014).
- [27] M. T. Quintino, J. Bowles, F. Hirsch, and N. Brunner, *Phys. Rev. A* **93**, 052115 (2016).
- [28] E. Bene and T. Vértesi, *New J. Phys.* **20**, 013021 (2018).
- [29] T. Temistocles, R. Rabelo, and M. T. Cunha, *Phys. Rev. A* **99**, 042120 (2019).
- [30] S.-L. Chen, N. Miklin, C. Budroni, and Y.-N. Chen, *Phys. Rev. Research* **3**, 023143 (2021).
- [31] S. López-Rosa, Z.-P. Xu, and A. Cabello, *Phys. Rev. A* **94**, 062121 (2016).
- [32] N. D. Mermin, *Phys. Rev. Lett.* **65**, 1838 (1990).
- [33] A. Acín, T. Durt, N. Gisin, and J. I. Latorre, *Phys. Rev. A* **65**, 052325 (2002).
- [34] C. Erven, E. Meyer-Scott, K. Fisher, J. Lavoie, B. L. Higgins, Z. Yan, C. J. Pugh, J.-P. Bourgoin, R. Prevedel, L. K. Shalm, L. Richards, N. Gigov, R. Laflamme, G. Weihs, T. Jennewein, and K. J. Resch, *Nat. Photon.* **8**, 292 (2014).
- [35] H. S. Poh, S. K. Joshi, A. Cerè, A. Cabello, and C. Kurtsiefer, *Phys. Rev. Lett.* **115**, 180408 (2015).
- [36] H. Anwer, M. Nawareg, A. Cabello, and M. Bourennane, *Phys. Rev. A* **100**, 022104 (2019).
- [37] B. P. Lanyon, M. Zwerger, P. Jurcevic, C. Hempel, W. Dür, H. J. Briegel, R. Blatt, and C. F. Roos, *Phys. Rev. Lett.* **112**, 100403 (2014).
- [38] D. Singh, Arvind, and K. Dorai, *J. Magn. Reson. O.* **10-11**, 100058 (2022).
- [39] C. Śliwa, *Phys. Lett. A* **317**, 165 (2003).
- [40] I. S. Oliveira, T. J. Bonagamba, R. S. Sarthour, J. C. C. Freitas, and E. R. deAzevedo, *NMR Quantum Information Processing* (Elsevier, Linacre House, Jordan Hill, Oxford OX2 8DP, UK, 2007).
- [41] D. G. Cory, M. D. Price, and T. F. Havel, *Physica D* **120**, 82 (1998), proceedings of the Fourth Workshop on Physics and Consumption.
- [42] A. Singh, D. Singh, V. Gulati, K. Dorai, and Arvind, *Eur. Phys. J. D* **74**, 168 (2020).
- [43] Z. Tošner, T. Vosegaard, C. Kehlet, N. Khaneja, S. J. Glaser, and N. C. Nielsen, *J. Magn. Reson.* **197**, 120 (2009).
- [44] T. Schulte-Herbruggen, R. Marx, A. Fahmy, L. Kauffman, S. Lomonaco, N. Khaneja, and S. J. Glaser, *Proc. Roy. Soc. A* **370**, 4651 (2012).
- [45] A. Gaikwad, K. Shende, Arvind, and K. Dorai, *Sci. Rep.* **12**, 3688 (2022).
- [46] G. Vidal and R. F. Werner, *Phys. Rev. A* **65**, 032314 (2002).
- [47] W. K. Wootters, *Phys. Rev. Lett.* **80**, 2245 (1998).